Radiative and continuum dampings of reversed shear Alfvén eigenmodes and perturbative analysis limitations for tokamaks

N. N. Gorelenkov [1],†, **L. Yu**[2], **Y. Wang**[3] and **G.-Y. Fu** [3]

[1]Princeton Plasma Physics Laboratory, P.O. Box 451, Princeton, NJ 08543-0451, USA

[2]School of Physics, East China University of Science and Technology, Shanghai 200237, PR China

[3]Institute for Fusion Theory and Simulation and School of Physics, Zhejiang University, Hangzhou 310027, PR China

A careful theoretical analysis of the excitation of Alfvén eigenmodes (AEs), such as TAE (toroidicity-induced AE) and RSAE (reversed shear AE), by superalfvenic energetic particles is required for reliable predictions of energetic ion relaxation in present day fusion experiments. This includes the evaluation of different AE damping mechanisms including radiative and continuum dampings which are the focus of this study. A recent comprehensive benchmark of different eigenmode solvers including gyrokinetic, gyrofluid and hybrid magenetohydrodynamics (MHD) has shown that employed models may have deficiencies when addressing some of them (Taimourzadeh *et al.*, *Nucl. Fusion*, vol. 59, 2019, 066006). In this paper, we are studying the radiative and continuum dampings of RSAEs in details which were missing in hybrid NOVA/NOVA-C calculations to prepare a NOVA-C package with a substantial upgrade. Both dampings require the finite Larmor radius (FLR) corrections to AE mode structures to be accounted for. Accurately calculating different damping rates and understanding their parametric dependencies, we resolve the limitation coming out of the perturbative approach. In particular, here, the radiative damping is included perturbatively, whereas the continuum damping is computed non-perturbatively. Our comparison leads to the conclusion that the non-perturbative treatment of the unstable RSAE modes is needed to find the agreement with the gyrokinetic calculations. We expect that the RSAE mode structure modification plays a dominant role in determining the RSAE stability.

Key words: fusion plasma, plasma waves, plasma instabilities

---

1. Introduction

Low-frequency Alfvén eigenmodes (AEs) could be dangerous for a controlled thermonuclear reactor due to their potentially deleterious effects on energetic ion (or energetic particle; EP) confinement, in particular, because they are driven by the EP population itself, and can lead to significant EP radial transport and losses in present day and in future fusion devices (Gorelenkov, Pinches & Toi 2014). They are opposite

† Email address for correspondence: ngorelen@pppl.gov

to high, sub-cyclotron frequency instabilities of compressional AEs or global AE modes considered elsewhere which are driven primarily by the energy gradient of the EP distribution function (Gorelenkov 2016). As a result, such radial transport can affect the plasma heating profiles and lead to localized EP losses to the first wall, potentially damaging the vacuum vessel. Instabilities of various low-frequency modes were predicted to be unstable in the International Thermonuclear Experimental Reactor (ITER) (Pinches *et al.* 2015) and will likely result in simultaneous multiple excitations with relatively high toroidal mode numbers although toroidicity-induced AE (TAE) frequency modes may result in a weak radial transport if the plasma microturbulence is ignored (Fitzgerald *et al.* 2016; Schneller *et al.* 2016; Gorelenkov *et al.* 2024). However, the AE amplitudes as well as the radial transport could be strongly enhanced if the microturbulence is included by broadening the resonances between the AEs and energetic particles (Gorelenkov & Duarte 2021).

Operational regimes when multiple unstable AEs are excited in present day devices, such as DIII-D tokamak where neutral-beam injected (NBI) ions are super-Alfvénic and capable of AE excitation, are of interest for the fusion community (Heidbrink & White 2020). In recent experiments on that device, plasma operation regimes were found with the characteristic EP profile resiliency or with a stiffness against an increasing NBI power (Collins *et al.* 2016). In those, so-called, critical gradient experiments, it was shown that beyond a certain injection power, the beam ions maintain approximately the same radial pressure profiles which do not depend on the increasing beam power.

It was also found that above the 'critical' level of NBI heating power, the background thermal ion temperature does not increase in time. At the same time, the underlying Alfvénic modes exhibit a rapid increase of their amplitudes above the instability threshold. The simulations of fusion plasmas require sophisticated models for AE stability for those regimes, which demand the accurate modelling of all AE damping and driving mechanisms. A representative collection of codes appeared in a recent dedicated article (Taimourzadeh *et al.* 2019) ranging from gyrokinetic to gyrofluid and to hybrid MHD/kinetic, which demonstrated overall a relatively good agreement among themselves in predicting such AE properties as the spacial structure and their stability properties.

We would like to point out one particularly promising research direction for predictions of the EP profile relaxation. It relies on the reduced and presently perturbative AE stability modelling, where the fast-ion transport is described by the quasi-linear (QL) methodology employed by the resonant-broadened QL code (RBQ) (Gorelenkov *et al.* 2019). In RBQ, the EP diffusion in the presence of multiple AEs is computed to evolve the fast-ion distribution function in the constant of motion space (COM) (Kaufman 1972). The COM implementation of QL equations at present is based on the perturbative treatment of the AEs. The formulation for the QL theory employed in RBQ has been greatly improved recently by including the resonant window function as well as the convective coefficients, which allows for a more accurately evaluation of the fast-ion characteristic motion near the resonances with the Alfvénic modes responsible for fast-ion transport (Duarte *et al.* 2023).

Qualitatively, the non-perturbative treatment of fast-ion-driven instabilities is required to describe phenomena which do not exist or are strongly modified from the case when the AE excitation is weak. However, often, the perturbative approach to describe those phenomena and, in particular, AE instabilities is sufficient to analyse their frequency and the mode structure. In fact, many pioneering studies of TAEs, RSAEs and other AEs were done using the perturbative methodology (we cite only a few relevant papers, Turnbull *et al.* 1993; Nazikian *et al.* 2003; Van Zeeland *et al.* 2007). One example of the non-perturbative solution is the energetic particle driven modes or EPMs. They

are considered in detail by Gorelenkov *et al.* (2014, see § 4.2.8) (in addition, the non-perturbative approach to AE excitation is discussed by Lauber 2013).

In this paper, the non-perturbative treatment of the damping has to do with the RSAE mode structure changing significantly depending on the value of the ion finite Larmor radius (FLR). This is considered in § 2. For the purpose of our analysis, both the mode structure and its growth rates change significantly which is the characteristic property of the non-perturbative RSAE mode. This seems to be the case relevant for the RSAE excitation in DIII-D experiments (Collins *et al.* 2016) of interest.

It follows from our analysis that for the models, such as RBQ, often one needs to rely on AE mode structures which are represented realistically or, in other words, computed non-perturbatively. As a result, these structures are expected to modify the AE eigenfrequencies and structures in response to changing plasma parameters when the instability evolves in time. Even though the perturbative treatment provides great insights into the development of the AE theory, it may not be sufficient to capture the details of specific damping mechanisms affecting AE stability properties. For example, the AE continuum damping developed using the perturbative approach (Berk *et al.* 1992) does not necessarily agree with more realistic, non-perturbative calculations (Taimourzadeh *et al.* 2019). This was shown by Bowden *et al.* (2014), where the kinetic extension of NOVA to include the continuum damping does not converge in the considered case.

Another important point to consider is that the aforementioned agreement between the gyrokinetic codes was found to have the coefficients of variation of growth rate values $CV_\gamma = 16, 17\%$ for $n = 4, 5$ (Taimourzadeh *et al.* 2019). Even though that number seems to be reasonably small, it could lead to a rather significant modification of the AE amplitude, A. Indeed, it follows from Gorelenkov & Duarte (2021, figure 3) and from Ghantous, Berk & Gorelenkov (2014, figure 7) that near threshold regimes, such variations of the growth rate could lead to rather significant variations in AE amplitudes. As a result, the diffusion coefficients of AE-driven fast-ion transport can increase dramatically since they are $\propto A^2$. The reason for the variation of the growth rates among the gyrokinetic codes is not clear since there were no data available on the values of the damping rates. Our study provides an ultimate assessment of different damping mechanisms to understand the discrepancy primarily in the RSAE decrements given that we can resolve each damping separately.

Taimourzadeh *et al.* (2019) performed the validation among eight numerical codes focussing on the stability of TAE and RSAEs in critical gradient experiments of DIII-D tokamak. A summary of those studies is given in figure 1.

The figure depicts the dependence of the net growth rates, γ_L, of the unstable RSAE modes on their toroidal mode number, n. While all the gyrokinetic codes compute γ_L rolling over n beyond $n = 5$, the perturbative, NOVA-C (Gorelenkov, Cheng & Fu 1999) growth rates show that the overall γ_L keeps increasing its value as n grows. To use NOVA-C results reliably in future predictive calculations, such as in QL RBQ (Gorelenkov *et al.* 2019), one needs to understand its limitations, which is the goal of our study. Another motivation of our work is to extend the radiative damping model of NOVA-C to RSAEs (Yu, Fu & Sheng 2009), which has to be done using different formulation than the TAE's radiative damping adopted by NOVA-C (Fu *et al.* 1996). In that paper, it was shown that the TAE radiative damping alongside with the ion Landau damping are two dominant dampings affecting TAE stability in Tokomak Fusion Test Reactor (TFTR) experiments.

Despite the differences in the approaches of different models used in the comparison, the obtained results allow the important conclusion to be made that the non-perturbative treatment could be the key factor to understand those differences. One particular source of disagreement, as pointed out by Taimourzadeh *et al.* (2019), comes from NOVA-C
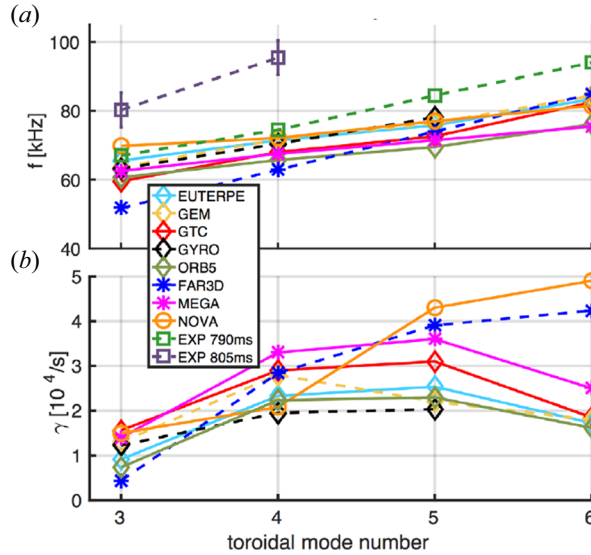
FIGURE 1. Linear stability analysis of $n = 3$–6 RSAE eigenmodes observed in DIII-D shot #159243 at 805 m (adopted from Taimourzadeh *et al.* 2019). (*a*) Real frequencies of RSAE and (*b*) computed net growth rates, γ_L, by eight codes. The plot markers are diamond, star and circle for the gyrokinetic, kinetic-MHD hybrid and perturbative eigenvalue codes, respectively.

perturbative simulations where each damping mechanism is treated separately. NOVA-C is the only code in that comparison which treats the growth and damping rates perturbatively. Other codes are gyrokinetic with two exceptions, MEGA being the initial value hybrid ideal MHD with gyrokinetic fast ions and FAR3D being the gyrofluid code. Note that the FAR3D curve also deviates from the gyrokinetic results likely due to using a Padé approximation for FLR corrections. Two important damping mechanisms, due to FLR effects of thermal and suprathermal beam ions, were ignored in NOVA-C. They are the radiative and continuum dampings, which can contribute to the growth rate deficit. Both are coming from thermal ion FLR corrections to TAE (Fu *et al.* 1996; Fu, Berk & Pletzer 2005) and RSAE (Yu *et al.* 2009) mode structures and eigenfrequencies.

The radiative damping is introduced through small spatial scale eigenstructure variations in the radial direction which, in their turn, are driven by the large-scale MHD structures locally exciting the kinetic Alfvén waves (KAWs) (Mett & Mahajan 1992).

The second damping emerges when the AE eigenfrequency resonates with the ideal MHD continuum (Berk *et al.* 1992; Chu *et al.* 1994). It is also due to KAW/AE coupling but coming through the direct energy flux from the global AE solution to the localized KAW at the Alfvén continuum. The continuum damping is expected to be strong under certain conditions, for example, when the toroidal rotation is high and when the AE global eigenmode structure has finite value at the resonance point with the continuum (Berk *et al.* 1992). As it follows from our analysis, such damping needs to rely on the non-perturbative methods (Chu *et al.* 1994).

In this paper, we compare different approaches to two important AE damping mechanisms, radiative and continuum, to choose the most optimal path forward for NOVA-C modifications. In addition to the NOVA-C code, we will be using the KAEC code capable of resolving the FLR effects on the AE mode structure (Yu *et al.* 2009), which will be discussed in detail in § 3.

2. Theoretical model

For further consideration, it is worth mentioning that both Alfvén mode radiative and the continuum dampings are related to each other (Fu *et al.* 2005). Both are due to KAW modifications of AE mode structure and eigenfrequency. AEs of interest, such as TAEs, RSAE, BAEs (Beta-induce Alfvén Eigenmode) or BAAEs (Beta-induce Alfvén Acoustic Eigenmode), have nominally global spacial mode structures meaning that their characteristic wavevectors satisfy $k_\perp \rho_i \ll 1$ and are smaller than the corresponding inequality related to fast ions $k_\perp \rho_b > 1$. The similarity in those mechanisms means that they are described by the same physics and mathematically by the same terms in the eigenmode equations.

To simulate this problem, one has to solve the Alfvén eigenmode equation numerically, which includes the FLR effects of thermal and fast ions, ion acoustic gyroradius and the finite parallel electric field terms (Fu *et al.* 2005; Yu *et al.* 2009). The eigenmode equation has the following form:

$$\nabla \cdot \left(\frac{\omega^2}{v_A^2} \nabla_\perp U \right) + \boldsymbol{B} \cdot \nabla \left(\frac{1}{B^2} \nabla \cdot B^2 \nabla_\perp Q \right) - \nabla \left(\frac{\mathrm{J}_\parallel}{B} \right) \cdot \nabla Q \times \boldsymbol{B}$$
$$+ 2 \frac{\boldsymbol{\kappa} \cdot \boldsymbol{B} \times \nabla \delta P}{B^2} + \nabla_\perp^2 g_{\mathrm{km}} \frac{1}{\rho} \nabla_\perp \rho \cdot \nabla_\perp U = 0, \tag{2.1}$$

with the following definitions:

$$Q = \frac{1}{B} \boldsymbol{b} \cdot \nabla U, \tag{2.2}$$

$$\delta P = \frac{1}{B} \boldsymbol{b} \times \nabla U \cdot \nabla P + \frac{2 \Gamma_{\mathrm{eff}} P \nabla U \cdot \boldsymbol{b} \times \boldsymbol{\kappa}}{B}, \tag{2.3}$$

$$g_{\mathrm{km}} = \frac{\omega^2}{v_A^2} \left(\frac{3}{4} \rho_i^2 + \frac{3}{4} \frac{n_b}{n_e} \frac{\rho_b^2}{1 + k_\perp^2 \rho_b^2} \right) (1 - \mathrm{i}\delta_i) + \rho_A^2 k_{\parallel m}^2 (1 - \mathrm{i}\delta_e), \tag{2.4}$$

where $U = -\int \phi \, \mathrm{d}t$, ϕ is the scalar potential of the fluctuation, ρ is the mass density, $\Gamma_{\mathrm{eff}} = (1 + 7T_i/4T_e)/(1 + T_i/T_e)$ is the effective specific heat index, $\rho_i = (m_i T_i)^{1/2}/eB$ and $\rho_b = (m_b T_b)^{1/2}/e_b B$ are the thermal and the beam ion gyroradii, $n_{e,b}$ is the plasma electron/beam ion density, $k_\perp$ is the perpendicular wave number of the mode, $\rho_A = (m_i T_e)^{1/2}/eB$ is the ion acoustic gyroradius, and $\delta_{i,e}$ is the resistivity due to ion and electron, respectively.

In (2.4), the beam ion kinetic FLR contributions are included via the Padé approximation expressions to account for the experimentally relevant regimes when $k_\perp \rho_b \geq 1$ (Kuvshinov 1994). The FLR relevant terms in our model appear non-perturbatively in the g_{km} expression, which resolves singularities at the points where the mode structures intersect the Alfvén continuum location or, in other words, where the AE resonates with the continuum.

It is through the g_{km} term that the RSAE radial structure is modified in a non-perturbative manner. There is an essential difference between the FLR effects on RSAE and on TAE structures. In theory and in numerical simulations, when TAE interacts with the Alfvén continuum or with KAW to dissipate (or radiate) its energy, the radial structure of the TAE eigenmode is still consistent with the MHD description (Berk *et al.* 1992; Lauber, Günter & Pinches 2005), i.e. it has the same global scale MHD structure between the points of the resonance with the continua, so that the radiative damping is merely a small-scale length perturbation of AE mode MHD structures (Lauber *et al.* 2005).

RSAEs were shown to have strong interaction with the KAW at the resonant points with the Alfvén continuum (Yu *et al.* 2009; Gorelenkov, Kramer & Nazikian 2011). We find a similar effect here, as presented in the next section.

One can see that thermal ion FLR effects, the first term in the first bracket of (2.4), and the fast-ion FLR effects, the second term in that bracket, both give rise to the AE damping through the thermal ion resistivity, δ_i. It is expected that the resulting continuum damping is insensitive to its value. Another part of the AE damping rate arises from the combination of the acoustic gyroradius and electron resistivity, $\mathrm{i}\delta_e$, see Yu *et al.* (2009) for more details.

In this model, the radiative damping and the continuum damping, if present, appear for the Alfvén eigenmode problem in the same way numerically. Both are included in simulations, however, in the cases when the AE mode frequency does not intersect the Alfvén continuum, the radiative damping is the only non-zero damping, whereas the continuum damping vanishes.

In the opposite case, i.e. when the AE resonates with the Alfvén continuum, the radiative damping dominates in the part of the region of smooth global mode structure, i.e. away from the resonant points. The continuum damping cannot be ignored at the resonant points. In the following, the RSAE dampings of the DIII-D discharge of interest are calculated according to this model. That is, in the region away from the resonance with the continuum, we treat the damping as the radiative damping, whereas at the resonance points, the damping is treated as the continuum damping.

3. RSAE continuum damping

Let us consider first the continuum damping of RSAEs. We apply the methodology described in § 2 to recent analysis of the aforementioned critical gradient experiments summarized in figure 1 (Taimourzadeh *et al.* 2019). To explore the properties of RSAE radiative and continuum dampings, we use the numerical code KAEC (Yu *et al.* 2009), which is based on the eigenmode equations presented above. The application of the KAEC code is warranted by its flexibility in studying the FLR corrections to the ideal MHD equations in both perturbative and non-perturbative regimes. That capability is instrumental in determining the venue for NOVA future modifications, which is one of the goals of this paper. KAEC does not have the advanced fast-ion physics present in NOVA-C (Gorelenkov *et al.* 1999), but has an important difference that it can treat the AE mode structure accounting for such effects as thermal ion FLR, see (2.1).

Since both dampings were missing in the NOVA-C analysis of Taimourzadeh *et al.* (2019) in applications to RSAEs, we need to understand the importance of each and whether those damping's perturbative treatment is appropriate for future NOVA-C development and applications (Gorelenkov *et al.* 2019).

The second important damping mechanism to consider is radiative, which was one of the dominant damping mechanisms for TAE stability in TFTR (Fu *et al.* 1995). It is included in the NOVA-C code (Fu *et al.* 1996). It was verified against LIGKA and LEMan gyrokinetic codes (Borba *et al.* 2010), although in NOVA-C simulations, the radiative damping was not separated from the continuum damping. The radiative damping model of LIGKA and LEMan codes applied to $n = 3$ TAE indicate that the damping is not localized at the location of the resonance with the Alfvén continuum, which is a characteristic signature of the radiative damping mechanism (Berk, Mett & Lindberg 1993; Fu *et al.* 1996).

We use the same plasma profiles as Taimourzadeh *et al.* (2019) and as presented in figure 2. One can notice that the fast-ion pressure exceeds the core plasma pressure significantly although only a small group of resonant beam ions contribute to AE excitations resulting in a relatively small AE growth rate, $\gamma/\omega \leq 5\,\%$, across the analysed and observed unstable eigenmodes.
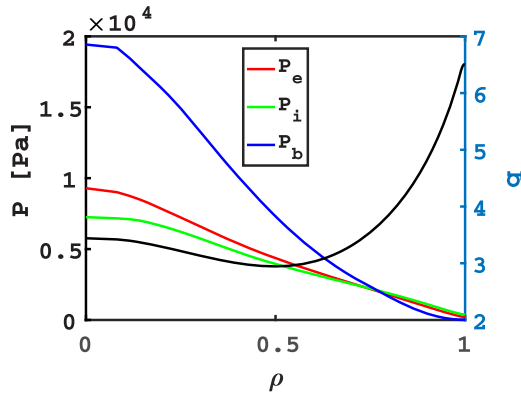
FIGURE 2. Pressure profiles of beam ions (blue), electrons (red) and thermal ions (green) of #159243 DIII-D shot. The black line is the safety factor profile with the right vertical axis.
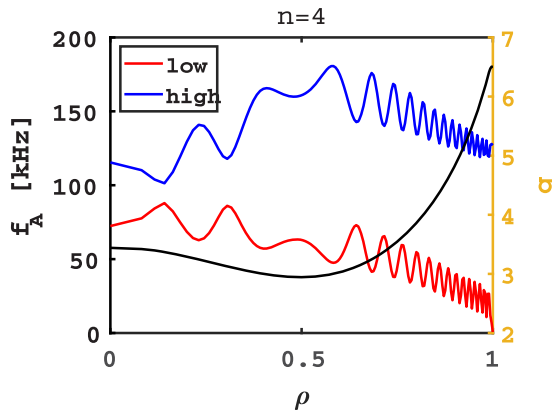

FIGURE 3. Alfvén continuum spectrum for toroidal mode number $n = 4$ as found by KAEC and expressed in kHz.

Figure 3 shows the $n = 4$ TAE gap continuum structure obtained in the so-called slow-sound approximation (Chu *et al.* 1992) when the interaction with the acoustic branch of the continuum is reduced to the upshift of the Alfvénic continuum (Gorelenkov *et al.* 2007) by the geodesic acoustic mode (GAM) frequency and when the acoustic continuum contributions are neglected. It is clear from this figure that the accumulation point of the $n = 4$ Alfvén continuum emerges at the minor radius $\rho = \sim 0.5$. At that location, RSAE is 'trapped' between the $m = 12$ harmonic of the Alfvén continuum according to the theory and the subsequent numerical analysis (Breizman *et al.* 2003).

We apply the KAEC to find the RSAE mode structures presented in figures 4–7, where each found eigenmode contains three dominant poloidal harmonics $m = 3n, 3n \pm 1$ ($q_{min} = 2.95 \simeq 3$) for each mode found without, panel (*a*), and with FLR small corrections at $\rho_i/a = 5 \times 10^{-4}$, panel (*b*). In the DIII-D plasma of interest, we have $\rho_i/a = 5.4 \times 10^{-3}$ (Taimourzadeh *et al.* 2019). RSAE mode structures shown in panel (*a*) are consistent with the structures of RSAEs found by the NOVA code, see Taimourzadeh *et al.* (2019, figures 5 and 6). NOVA solutions reported in that paper exhibit similar singularities in the RSAE structures at the resonances with the ideal MHD continuum, figures 4–7(*a*).
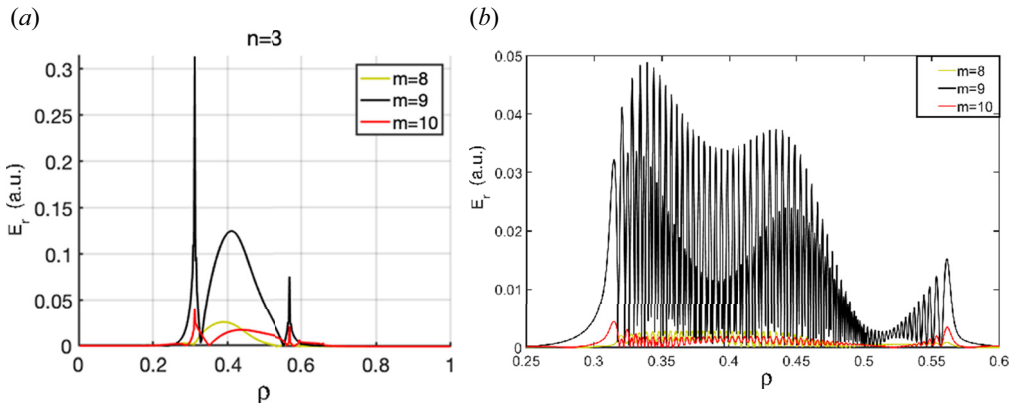
FIGURE 4. Mode structure of $n = 3$ RSAEs found by the KAEC code in DIII-D shot #159243 under (*a*) the ideal MHD limit and (*b*) the limit of small FLRs, $\rho_i/a = 5 \times 10^{-4}$.
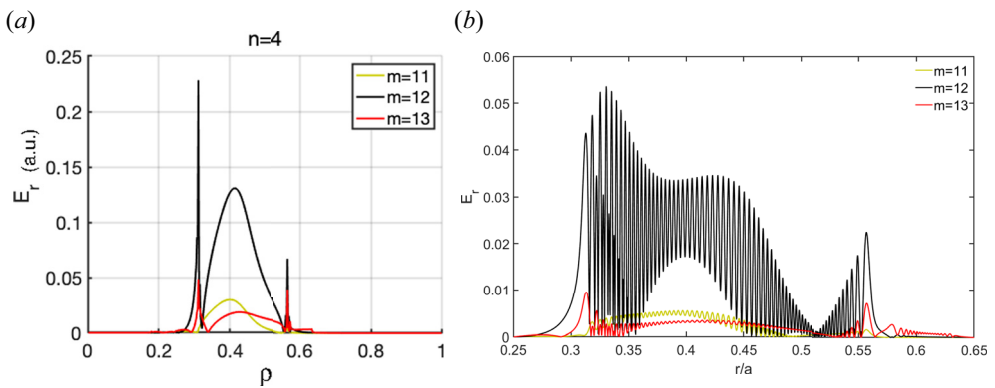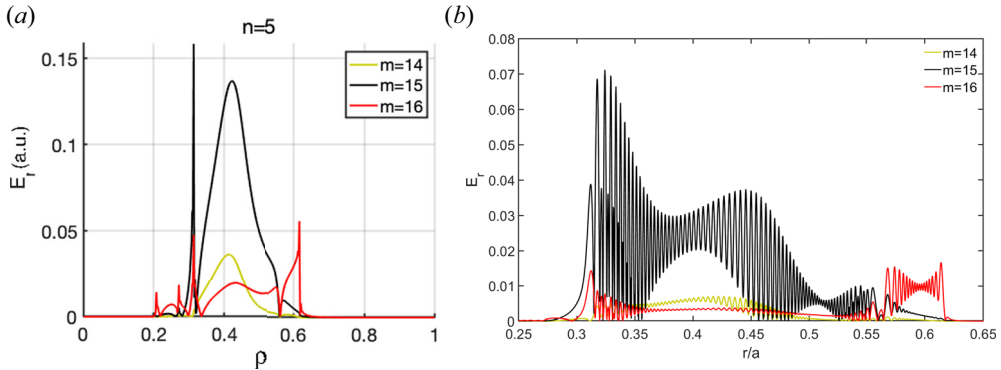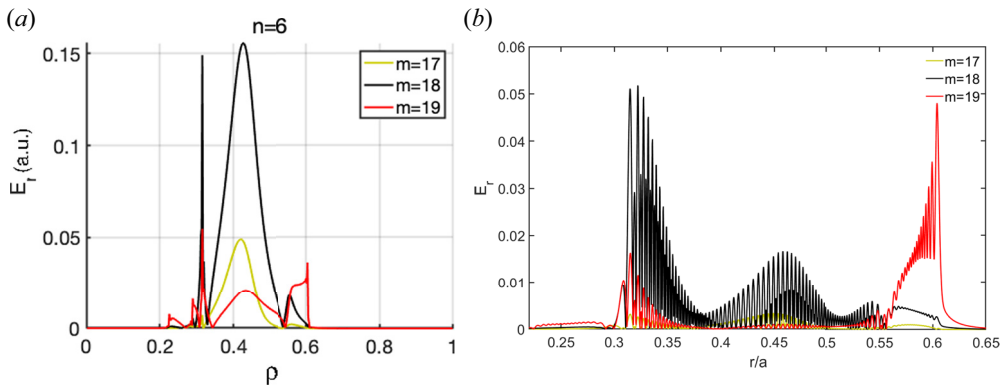

FIGURE 5. The same as in figure 4 but for $n = 4$.

RSAEs calculated using the KAEC simulations had $N = 800$ radial grids for panel (*a*) and $N = 2001$ radial points for panel (*b*).[1]

It follows from the formulation of the RSAE radiative damping, (4.1), that it vanishes if FLR effects of thermal and beam ions go to zero. The continuum damping found this way is presented in figure 11 as a dash-dotted curve shown as a function of the corresponding eigenmode toroidal mode number.

In figures 4(*b*)–7(*b*), significant non-perturbative alterations in the RSAE mode structures are evident, attributable to plasma ion FLR effects. Notably, the mode structures exhibit radial oscillations, indicative of the pronounced influence of the KAW on MHD coupling. This contrasts with the earlier demonstrated TAE modification, which retains

---

[1]Ideal MHD is a powerful tool available for the analysis of such phenomena as low-frequency Alfvénic oscillations. However, we would like to bring the reader's attention to the potential theoretical and numerical misinterpretation which could arise if the damping of the low-frequency modes is completely ignored. This is explained in applications to the so-called Alfvén slow eigenmodes (ASEs) in detail by Gorelenkov & Berk (2021). ASEs are well-damped modes due to strong interactions with the acoustic continuum and, as a result, strong thermal ion Landau damping. In contrast to that treatment, a detailed study of the same modes should be of interest (Rodrigues & Cella 2021). In the later work, the high-order geodesic-acoustic eigenmodes (HOGAEs) were singled out from numerical simulations because they had small ion Landau damping which was computed by the CASTOR-K code (Borba & Kerner 1999).

FIGURE 6. The same as in figure 4 but for $n = 5$.

FIGURE 7. The same as in figure 4 but for $n = 6$.

its global MHD-like structure with relatively minor modifications by the KAW solution (Lauber *et al.* 2005).

Here, we illustrate the variation of RSAE structures for a single toroidal mode number. This is depicted in figure 8(a–c) for $n = 4$ RSAE, in addition to figure 5(b). The identified RSAE solutions indicate that the dominant component of the mode structure is formed by its KAW part, primarily due to the eigenfrequency's proximity to the Alfv'en continuum. This stands in contrast to the gyrokinetic RSAE solution presented by Taimourzadeh *et al.* (2019), where the RSAE eigenfrequency lies above the continuum, resulting in a weaker contribution from the KAW. This observation is supported by the RSAE growth rate versus n dependence depicted in figure 11, where contributions from the continuum and radiative dampings are relatively small compared with the beam ion drive.

Now, let us compare the model outlined above in § 2 with another published model, namely the resistive MHD model (Borba & Kerner 1999) (although in CASTOR-K, the 'complex resistivity' is used). The latter is able to evaluate the continuum damping of various AEs. According to the resistive MHD, the calculated damping comprises the resistive component and its continuum counterpart. The resistive damping decreases with the resistivity, whereas the continuum part is independent of the resistivity.

As the plasma resistivity asymptotically approaches zero with ρ_i going to zero, the remaining part of the overall damping approaches the continuum damping. Our model
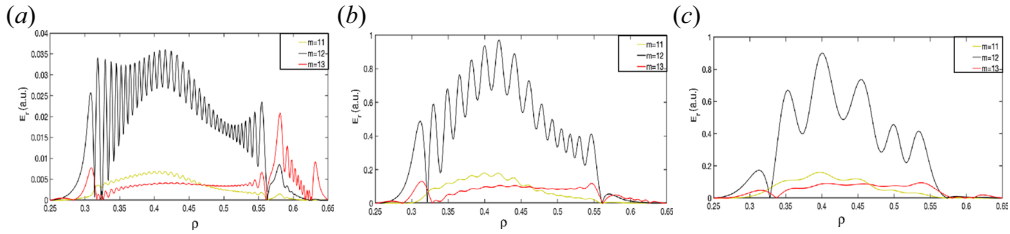
FIGURE 8. Mode structures of $n = 4$ RSAEs found by the KAEC code in DIII-D shot #159243 when ion FLR effects are included non-perturbatively: (*a*) $\rho_i/a = 10^{-3}$, $\gamma/\omega = -0.0191$, $\omega/\omega_A = 0.14986$; (*b*) $\rho_i/a = 2.5 \times 10^{-3}$, $\gamma/\omega = -0.0168$, $\omega/\omega_A = 0.15029$; (*c*) $\rho_i/a = 7 \times 10^{-3}$, $\gamma/\omega = -0.0144$, $\omega/\omega_A = 0.15343$. Here, $\omega_A = 2\pi(478\,(\text{kHz}))$.
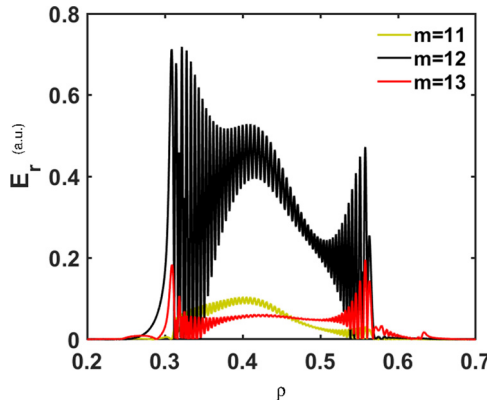

FIGURE 9. Mode structure of $n = 4$ RSAE (shown here) is similar to that in figure 5 except that it is obtained for the kinetic term of the eigenmode equation (3.1) set to a smaller value: $\delta = 2.5 \times 10^{-8}$.

is expandable to the framework of the resistive MHD via the modification of the term g_{km} in the following way:

$$g_{\text{km}} = -\mathrm{i}\delta \frac{\omega^2 a^2}{v_A^2}, \tag{3.1}$$

where δ is the effective resistivity parameter, v_A is the Alfvén velocity. For the consistency of our analysis, we present the derivation of (3.1) in Appendix A.

Within the resistive MHD framework, we find $n = 4$ RSAE whose poloidal harmonic's radial structures are depicted in figure 9 for the number of radial grid points $N = 2001$. The similar mode structure is obtained earlier and is shown in figure 5(*b*). Almost identical mode structures imply that the same RSAEs solution is found by the two methods. The resistive framework of (3.1) includes the artificial resistivity parameter δ which was fixed at 2.5×10^{-8}. As we mentioned, only the continuum damping survives when the resistivity parameter vanishes.

Employing the same resistive MHD model, let us study the RSAE eigenfrequency and continuum damping dependencies on the mode toroidal mode number. Figure 10 (solid line) plots the real frequencies of RSAEs for the toroidal mode numbers in the range of interest $n = 3$–6 calculated by the KAEC code. Similar to the mode frequencies in figure 1 found by the ideal MHD code NOVA perturbatively, we have found that the RSAE frequencies span from 73 kHz to 81 kHz.
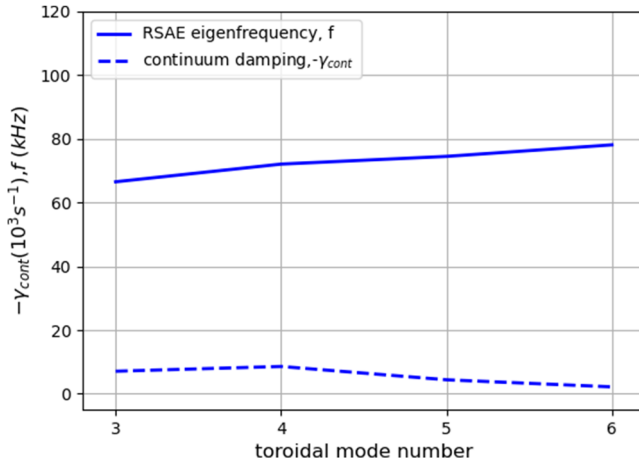
FIGURE 10. Real frequencies and the continuum damping rate of RSAEs with different toroidal mode numbers calculated using the resistive MHD formulations and the artificial resistivity parameter set to $\delta = 2.5 \times 10^{-8}$.
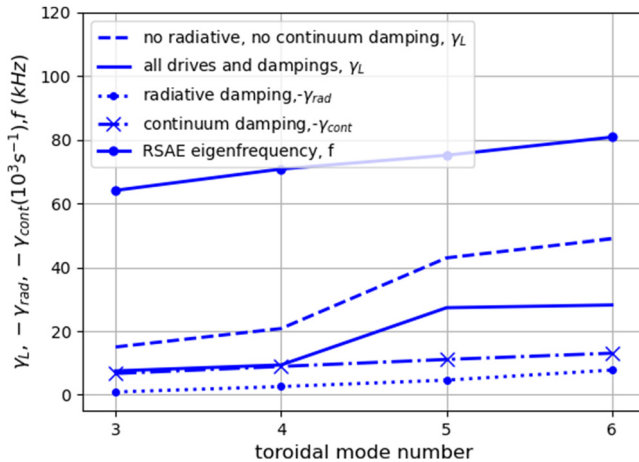

FIGURE 11. RSAE growth/damping rates with and without the radiative and continuum dampings as denoted. Dash-dotted blue line corresponds to the non-perturbative continuum damping of the modes shown in figures 4–7(b) as functions of their toroidal mode numbers n.

We would like to stress that in this paper, the obtained RSAE continuum dampings correspond to the non-perturbative calculations and are shown in figure 11 versus the toroidal mode number, n, $|\gamma_{\mathrm{cont}}| \sim n^2$. The values of the continuum damping increase with the toroidal mode number as expected since the eigenmode scalelength becomes smaller and the mode couples more strongly to the KAW at the resonance with the Alfvén continuum. However, the resistive MHD model calculations of RSAE continuum damping deviate from those of the non-ideal kinetic FLR model of KAEC. This is due to the simplification used for the g_{km} FLR term responsible for small-scale oscillations of the mode structure near the resonance with the continuum.

4. RSAE radiative damping

The radiative damping has been shown to limit the range of unstable TAEs in JET experiments (Aslanyan *et al.* 2019). Indeed, in that work, the TAE damping rates were simulated by the gyrokinetic code GTC non-perturbatively (Lin *et al.* 1998). Given the dependence of the radiative damping on the toroidal mode number, i.e. that it grows as $\gamma_{rad} \propto n^{1/3}$ at high n values (Mett & Mahajan 1992), we expect that it will be a strong stabilizing factor for AE instabilities in future big devices like ITER.[2] Thus, one of our goals is to evaluate the accuracy of existing expressions for the radiative damping of RSAEs and support those findings by calculations.

The expression of the radiative damping was extensively studied previously (Yu *et al.* 2009) by interpolating the numerical results into the expected exponential dependence,

$$\frac{\gamma_{rad}}{\omega} = S c_1 \exp\left(-\frac{c_2 S}{\sqrt{\Lambda}}\right), \tag{4.1}$$

where various plasma parameters entering the above expression are taken at the location of the safety factor at its minimum point, $q(r_{min}) = q_{min}$,

$$S = -mR q_{min}^2 k_{\parallel,min}(\omega^2 - \omega_A^2(r))/(\omega_A^2(r) r_{min}^2 q_{min}''), \tag{4.2}$$

$$\Lambda = q_{min} \rho_s^2 (m/r_{min})^4 (n q_{min}/m - 1)/q_{min}, \tag{4.3}$$

$$\rho_s^2 = \left(\frac{T_e}{T_i} + \frac{3}{4}\right) \rho_i^2 + \frac{3}{4} \frac{n_b}{n_e} \frac{\rho_b^2}{1 + k_\perp^2 \rho_b^2}, \tag{4.4}$$

where $k_\parallel$ is the parallel wave vector, ω is the RSAE frequency, $\rho_{i,b}$ are the thermal and beam ion Larmor radius, respectively, ρ_s is the effective Larmor radius (cf. Zonca *et al.* 2014), q_{min} is the safety factor at its minimum, $\omega_A(r)$ is the Alfvén continuum frequency, R is the toroidal plasma major radius, $q'' = \partial^2 q/\partial r^2$, r is the radial coordinate, and n_b and n_e are beam ion and electron densities, respectively.

We note that in (4.4), the beam ion contribution to the radiative damping is quantitatively and qualitatively different from the thermal ion contribution. For beam ions, it contains an additional factor $(1 + k_\perp^2 \rho_b^2)^{-1}$ which is a correction due to the perpendicular wave vector in the presence of superthermal beam ions (Kuvshinov 1994). It emerges from the Padé approximation used for the Bessel function, as shown by Pegoraro, Porcelli & Schep (1989). Moreover, one can notice that increasing the toroidal mode number, n, leads to the decrease of relative fast-ions contribution to the radiative damping. We also should note that for the most unstable RSAE solutions, lowest in frequency, the estimates for the radial wavevector can be done based on the formulation of the kinetic RSAEs (Gorelenkov *et al.* 2011). It was shown in that paper that the characteristic width of the mode is determined by the following expression:

$$\Delta r = \frac{4}{\pi} \frac{w^2}{r_0} \sqrt{\frac{\alpha \epsilon (q^2 - 1)}{q^2}}, \tag{4.5}$$

where w is the characteristic width of the low shear region, $w^2 = 2 q_{min}/q''|_{r=r_0}$ and $\alpha = -R_0 q_{min}^2 \beta'$. Based on that formula, it is straightforward to show that $k_\perp \simeq k_\theta \simeq m/r|_{q=q_{min}}$

---

[2]Pinches *et al.* (2015) found the radiative damping to be independent on n when n is large and shear is low. Our results show that at low n, we expect $\gamma_{rad} \propto n$, which follows from the dotted curve in figure 11. Such dependence may be attributed to low values of n which are important for present day conventional tokamaks, such as DIII-D (Taimourzadeh *et al.* 2019).

and that k_r can be ignored. This also follows from Taimourzadeh *et al.* (2019), where RSAE mode structures were obtained by different codes. From the comparison shown in figures 5 and 6 of that paper by 8 codes, the RSAE mode structure is characterized by the wavevector primarily directed in the poloidal direction.

Figure 11 compares the contributions of both continuum and radiative dampings to the linear growth rate of $n = 3$–6 RSAEs. It is interesting to observe that for this case, the contributions of both dampings of interest are very close to each other.[3] At the same time, the net growth rate with the inclusion of non-perturbative continuum damping and perturbative radiative damping still does not result in net growth rate rollover as one would expect based on the multiple non-perturbative studies shown in figure 3.

The case we considered is far from being marginal for RSAE stability. This is in contrast to ITER (Pinches *et al.* 2015), where fast-ion population pressure is not as strong as in DIII-D (Collins *et al.* 2016) considered here. As it follows from figure 2, the energetic particle pressure P_b is high in the DIII-D shot #159243 of interest, and almost equal to the sum of thermal electron pressure P_e and thermal ion pressure P_i in the plasma core. The safety factor profile is reversed below $r = 0.5a$, where a is the minor radius although the value of $q_{\min} = 3$ in #159243 discharge at the point of interest is higher than projected in ITER, $q_{\min} \gtrsim 1$.

5. Summary and discussions

Applying the perturbative and non-perturbative techniques, we evaluated two important damping rates for this problem: radiative and continuum, as well as their contributions to the total RSAE linear growth rate. We also compared them with the perturbative approach employed in NOVA-C, where the RSAE growth rates include several other kinetic damping rates. We have shown that in the considered case of the reversed magnetic shear plasma, the perturbative growth rates of RSAE modes are not compatible with the non-perturbative calculations reported earlier (Taimourzadeh *et al.* 2019). We found that NOVA-C growth rates have a similar, to that of the reference, dependence on the toroidal mode number for $n \le 5$. Nevertheless both, radiative and continuum, dampings added to the total growth rates do not lead to the rollover γ_L at high $n > 5$ values which was reported by the non-perturbative simulations. Qualitatively, this is due to the RSAE radial mode structure being relatively broad in comparison with the RSAEs found in gyrokinetic calculations (see Taimourzadeh *et al.* 2019, figure 5). This occurs not only because of broader dominant m's harmonics, but also because of the presence $m \pm 1$ poloidal sideband harmonics.

One potential consequence of RSAE fine structure we found is that it may elevate RSAE damping rate due to trapped electron collisional damping, γ_{ecoll}, considered earlier (Fu & Cheng 1992; Gorelenkov & Sharapov 1992) (and adopted for burning plasma conditions by Gorelenkov *et al.* 2003). This is because without the drive, the eigenmodes contain the small radial scale length due to interaction with KAW such as shown in figures 4–7(*b*) and 8. If this happens, the RSAE damping will increase. However, strong dependence of γ_{ecoll} on plasma parameters and, more importantly, its sensitivity to RSAE non-perturbative analysis require accurate study of γ_{ecoll} parametric dependence, which is beyond the scope of this paper. We should note here that Pinches *et al.* (2015) found that in applications to ITER, γ_{ecoll} was important near the plasma edge. In another study, (Gorelenkov *et al.* 2003), a similar conclusion was reached for ITER plasma where $\gamma_{\mathrm{ecoll}}/\omega < 1\,\%$ was found for TAE modes.

---

[3]This is in contrast to the analytic theoretical expectations for ITER (Pinches *et al.* 2015), where it was shown that with closed TAE gap in that device, the continuum damping will overcome the radiative one for TAE modes in the baseline scenario. We would like to comment that this is likely due to TAEs resonating with the continuum at the plasma edge where the safety factor shear is significant.

To estimate γ_{ecoll} for RSAEs, i.e. at $q_{\min}$ location where the magnetic shear is zero, $s = 0$, one can use Gorelenkov *et al.* (2003, (5) and (6)) with the depletion parameter set to $\sigma = 1$. The appropriate expression to use is

$$\frac{\gamma_{\text{ecoll}}}{\omega} = -\sqrt{\frac{\pi}{2}} \frac{1}{4} \mathrm{I}_2 q^2 \frac{8\beta_{pc}}{1+\sigma} \sqrt{\frac{\nu_e}{\omega - \omega_{\min}}} \left[\ln\left(16\sqrt{\frac{(\omega - \omega_{\min})\epsilon}{\nu_e}} \right) \right]^{-3/2}, \qquad (5.1)$$

where $\nu_e = 0.145(R_{[m]}q/x_i^3)B_{[10T]}^2/[(1 + \sigma/4)T_{e[10\,\text{keV}]}^3]$, and where the major radius R is given in m, the equilibrium magnetic field B in units 10T, T_e in 10 keV units and where for RSAEs driven by passing ions, we require at the resonance point $x_i = v_A(k_\parallel qR)/|k_\parallel qR \pm 1|v_i$. Also here, we added $\omega_{\min}$ which is the minimum RSAE frequency. It is interesting that zero shear location of RSAE negates the FLR related term in the full expression for γ_{ecoll} (cf. Gorelenkov *et al.* 2003, (5)).

It is clear that since the RSAE eigenfrequency contribution, $\omega - \omega_{\min}$, can go from close to zero value up to a TAE frequency related value, (5.1) can result in quite large γ_{ecoll}. Nevertheless, for DIII-D plasma, analysed in this paper, NOVA-C computed γ_{ecoll} to be less than 1 % for all the modes analysed (Taimourzadeh *et al.* 2019). This is likely due to a more accurate way to compute γ_{ecoll} implemented in NOVA-C, where the trapped electron perturbed distribution function is expanded in a Taylor series (Fu, Cheng & Wong 1993). Importantly, parametric dependence of (5.1) shows that fine FLR related structure effects disappear due to zero shear at $q_{\min}$.

In our simulations, non-perturbative RSAEs have broader radial mode structure due to FLR effects coming from interactions with KAWs. KAWs emerge from the Alfvén continuum which consist of essentially propagating KAWs structures. This needs to be compared with the solutions of gyrokinetic codes and with the ideal MHD code NOVA (Taimourzadeh *et al.* 2019). There, the EP drive is essential in determining the RSAE mode structure. It helps to understand why the elevated RSAE eigenfrequency is above the continuum to the level sufficient to form the MHD-like mode structure. Such non-perturbatively driven RSAEs exhibit strong deviation of their mode structure from MHD as well as from our stable RSAE structures.

What comes as a surprise to us is that the combined thermal plasma damping and beam drive have a relatively benign modification of the RSAE MHD structure, see RSAEs calculated by different codes reported by Taimourzadeh *et al.* (2019).

Our conclusions are important for understanding the direction of the potential improvements for the NOVA suit of codes which are required for predictive simulations of the advanced plasma scenarios with the reversed shear profiles.

Declaration of interests

The authors report no conflict of interest.

Appendix A. derivation of the FLR term g_{km}, (3.1)

The eigenmode equation with thermal ion FLR effects can be derived basing on the resistive MHD since the term g_{km} keeps only the imaginary part while ignoring the real part.

To be consistent with the normalized form of g_{km} used in the code KAEC where the gyro-radius ρ_i is normalized to the minor radius a and the frequency ω normalized to $v_A(0)/R_0$, we multiply (2.4) by the factor R_0^2/a^2, then obtain the modified expression of that equation:

$$\bar{g}_{km} = \left[\frac{\omega^2 R_0^2}{v_A^2} \left(\frac{3}{4} \frac{\rho_i^2}{a^2} + \frac{3}{4} \frac{n_b}{n_e} \frac{\rho_b^2/a^2}{1 + k_\perp^2 \rho_b^2} \right) (1 - \mathrm{i}\delta_i) + \frac{1}{2} \frac{\rho_A^2}{a^2} \left(n - \frac{m}{q} \right)^2 (1 - \mathrm{i}\delta_e) \right]. \quad (A1)$$

By keeping the imaginary part of (A1) to extend the model of the resistive MHD, we modify $\bar{g}_{km}$ in the following way:

$$\bar{g}_{km} = -\mathrm{i}\delta \frac{\omega^2}{v_A^2/R_0^2}, \quad (A2)$$

where δ is the effective resistivity parameter. We apply this form of $\bar{g}_{km}$ given by (A2) in the code KAEC. Here, δ is a small number and is chosen according to the gyro-radius, i.e. $\delta = \rho_i^2/a^2$ in our numerical computation.

With (A2) and the relation $\bar{g}_{km} = g_{km} R_0^2/a^2$, the formula for g_{km} becomes (3.1).

REFERENCES

ASLANYAN, V., TAIMOURZADEH, S., SHI, L., LIN, Z., DONG, G., PUGLIA, P., PORKOLAB, M., DUMONT, R., SHARAPOV, S.E., MAILLOUX, J., *et al.* 2019 Gyrokinetic simulations of toroidal Alfvén eigenmodes excited by energetic ions and external antennas on the joint European torus. *Nucl. Fusion* **59**, 026008.

BERK, H.L., METT, R.R. & LINDBERG, D.M. 1993 Arbitrary mode number boundary layer theory for nonideal toroidal Alfvén modes. *Phys. Fluids* B **5**, 3969.

BERK, H.L., VAN DAM, J.W., GUO, Z. & LINDBERG, D.M. 1992 Continuum damping of low-n toroidicity-induced shear Alfvén eigenmodes. *Phys. Fluids* B **4**, 1806–1835.

BORBA, D., FASOLI, A., GORELENKOV, N.N., GUNTER, S., LAUBER, P., MELLET, N., NAZIKIAN, R., PANIS, T., PINCHES, S.D., SPONG, D., *et al.* 2010 The influence of plasma shaping on the damping of toroidal Alfvén eigenmodes. In *Proceedings of 23rd IAEA Fusion Energy Conference, Daejeon, Republic of Korea*, pp. 1–8. IAEA.

BORBA, D. & KERNER, W. 1999 CASTOR-K: stability analysis of Alfvén Eigenmodes in the presence of energetic ions in Tokamaks. *J. Comput. Phys.* **153**, 101–111.

BOWDEN, G.W., KOENIES, A., HOL, M.J., GORELENKOV, N.N. & DENNIS, G.R. 2014 Comparison of methods for numerical calculation of continuum damping. *Phys. Plasmas* **21**, 052508.

BREIZMAN, B.N., BERK, H.L., PEKKER, M.S., PINCHES, S.D. & SHARAPOV, S.E. 2003 Theory of Alfvén eigenmodes in shear reversed plasmas. *Phys. Plasmas* **10**, 3649–3660.

CHU, M.S., GREENE, J.M., LAO, L.L., TURNBULL, A.D. & CHANCE, M.S. 1992 A numerical study of the high-n shear Alfvén spectrum gap and the high-n gap mode. *Phys. Fluids* B **4**, 3713–3721.

CHU, M.S., GREENE, J.M., LING, W., TURNBULL, A.D., BERK, H.L. & ROSEBLUTH, M.N. 1994 A numerical study of the Alfvén continuum damping of toroidal Alfvén eigenmodes. *Phys. Plasmas* **1**, 1214–1225.

COLLINS, C.S., HEIDBRINK, W.W., AUSTIN, M.E., KRAMER, G.J., PACE, D.C., PETTY, C.C., STAGNER, L., VAN ZEELAND, M.A., WHITE, R.B., ZHU, Y.B., *et al.* 2016 Observation of critical gradient behavior in Alfvén eigenmode induced fast-ion transport. *Phys. Rev. Lett.* **116**, 095001.

DUARTE, V.N., LESTZ, J.B., GORELENKOV, N.N. & WHITE, R.B. 2023 Shifting and splitting of resonance lines due to dynamical friction in plasmas. *Phys. Rev. Lett.* **130**, 105101.

FITZGERALD, M., SHARAPOV, S.E., RODRIGUES, P. & BORBA, D. 2016 Predictive nonlinear studies of TAE-induced alpha-particle transport in the $Q = 10$ ITER baseline scenario. *Nucl. Fusion* **56**, 112010.

FU, G.Y., BERK, H.L. & PLETZER, A. 2005 Kinetic damping of toroidal Alfvén eigenmodes. *Phys. Plasmas* **12** (8), 082505.

FU, G.Y. & CHENG, C.Z. 1992 Excitation of high-*n* toroidicity-induced shear Alfvén eigenmodes by energetic particles and fusion alpha particles in tokamaks. *Phys. Fluids* B **4**, 3722–3734.

FU, G.Y., CHENG, C.Z., BUDNY, R., CHANG, Z., DARROW, D.S., FREDRICKSON, E., MAZZUCATO, E., NAZIKIAN, R., WONG, K.L. & ZWEBEN, S. 1996 Analysis of alpha particle-driven toroidal Alfvén eigenmodes in Tokamak Fusion Test Reactor deuterium-tritium experiments. *Phys. Plasmas* **3**, 4036–4045.

FU, G.Y., CHENG, C.Z., BUDNY, R., CHANG, Z., DARROW, D.S., FREDRICKSON, E., MAZZUCATO, E., NAZIKIAN, R. & ZWEBEN, S. 1995 Stability analysis of toroidicity-induced Alfvén eigenmodes in TFTR deuterium-tritium experiments. *Phys. Rev. Lett.* **75**, 2336–2339.

FU, G.Y., CHENG, C.Z. & WONG, K.L. 1993 Stability of the toroidicity-induced Alfvén eigenmode in axisymmetric toroidal equilibria. *Phys. Fluids* B **5**, 4040–4050.

GHANTOUS, K., BERK, H.L. & GORELENKOV, N.N. 2014 Comparing the line broadened quasilinear model to vlasov code. *Phys. Plasmas* **21**, 032119.

GORELENKOV, N.N. 2016 Energetic particle-driven compressional Alfvén eigenmodes and prospects for ion cyclotron emission studies in fusion plasmas. *New J. Phys.* **18**, 105010.

GORELENKOV, N.N. & BERK, H.L. 2021 Comment on "Theory of Alfvén-slow frequency gaps and discovery of Alfvén-slow eigenmodes in tokamaks" [phys. plasmas 26, 082508 (2019)]. *Phys. Plasmas* **28** (07), 074701.

GORELENKOV, N.N., BERK, H.L., FREDRICKSON, E. & SHARAPOV, S.E. 2007 Predictions and observations of low-shear beta-induced shear Alfvén-acoustic eigenmodes in toroidal plasmas. *Phys. Lett.* A **370**, 70–77.

GORELENKOV, N.N., CHENG, C.Z. & FU, G.Y. 1999 Fast particle finite orbit width and Larmor radius effects on low-n toroidicity induced Alfvén eigenmode excitation. *Phys. Plasmas* **6**, 2802–2807.

GORELENKOV, N.N. & DUARTE, V.N. 2021 Microturbulence-mediated route for energetic ion transport and Alfvénic mode amplitude oscillations in tokamaks. *Phys. Lett.* A **386**, 126944.

GORELENKOV, N.N., DUARTE, V.N., COLLINS, C.S., PODESTÀ, M. & WHITE, R.B. 2019 Verification and application of resonance broadened quasi-linear (RBQ) model with multiple Alfvén instabilities. *Phys. Plasmas* **26** (07), 072507.

GORELENKOV, N.N., DUARTE, V.N., GORELENKOVA, M.V., PODESTA, M., LIN, ZH. & PINCHES, S.D. 2024 Fast ion relaxation in ITER mediated by Alfvén instabilities. *Nucl. Fusion* **64**, 076061.

GORELENKOV, N.N., FREDRICKSON, E.D., BELOVA, E., CHENG, C.Z., GATES, D., KAYE, S. & WHITE, R.B. 2003 Theory and observations of high frequency Alfvén eigenmodes in low aspect ratio plasmas. *Nucl. Fusion* **43**, 228–233.

GORELENKOV, N.N., KRAMER, G.J. & NAZIKIAN, R. 2011 Combined ideal and kinetic effects on reversed shear Alfvén eigenmodes. *Phys. Plasma* **18**, 102503.

GORELENKOV, N.N., PINCHES, S.D. & TOI, K. 2014 Energetic particle physics in fusion research in preparation for burning plasma experiments. *Nucl. Fusion* **54**, 125001.

GORELENKOV, N.N. & SHARAPOV, S.E. 1992 On the collisional damping of TAE-modes on trapped electrons in tokamaks. *Phys. Scr.* **45**, 163–166.

HEIDBRINK, W.W. & WHITE, R.B. 2020 Mechanisms of energetic-particle transport in magnetically confined plasmas. *Phys. Plasmas* **27**, 030901.

KAUFMAN, A.N. 1972 Reformulation of quasi-linear theory. *J. Plasma Phys.* **8** (1), 1–5.

KUVSHINOV, B.N. 1994 Magnetohydrodynamic model for plasma instabilities in the ion-kinetic regime. *Plasma Phys. Control. Fusion* **36**, 867.

LAUBER, P. 2013 Super-thermal particles in hot plasma-kinetic models, numerical solution strategies, and comparison to tokamak experiments. *Phys. Rep.* **533**, 33–68.

LAUBER, P., GÜNTER, S. & PINCHES, S.D. 2005 Kinetic properties of shear Alfvén eigenmodes in tokamak plasmas. *Phys. Plasmas* **12**, 122501.

LIN, Z., HAHM, T.S., LEE, W.W., TANG, W.M. & WHITE, R.B. 1998 Gyrokinetic simulations of toroidal Alfvén eigenmodes excited by energetic ions and external antennas on the joint European torus. *Science* **281**, 1835–1845.

METT, R.R. & MAHAJAN, S.M. 1992 Kinetic theory of toroidicity-induced Alfvén eigenmodes. *Phys. Fluids* B **4**, 2885–2893.

NAZIKIAN, R., KRAMER, G.J., CHENG, C.Z., GORELENKOV, N.N., BERK, H.L. & SHARAPOV, S.E. 2003 New interpretation of alpha-particle-driven instabilities in deuterium-tritium experiments on the tokamak fusion test reactor. *Phys. Rev. Lett.* **91**, 125003.

PEGORARO, F., PORCELLI, F. & SCHEP, T.J. 1989 Internal kink modes in the ion-kinetic regime. *Phys. Fluids* B **1**, 364–374.

PINCHES, S.D., CHAPMAN, I.T., LAUBER, P.W., OLIVER, H.J.C., SHARAPOV, S.E., SHINOHARA, K. & TANI, K. 2015 Energetic ions in ITER plasmas. *Phys. Plasmas* **22**, 021807.

RODRIGUES, P. & CELLA, F. 2021 High-order geodesic coupling of shear-Alfvén and acoustic continua in tokamaks. *Nucl. Fusion* **61**, 096001.

SCHNELLER, M., LAUBER, P., BRÜDGAM, M., PINCHES, S.D. & GÜNTER, S. 2016 Nonlinear energetic particle transport in the presence of multiple Alfvénic waves in ITER. *Plasma Phys. Control Fusion* **58**, 014019.

TAIMOURZADEH, S., BASS, E.M., CHEN, Y., COLLINS, C., GORELENKOV, N.N., KÖNIES, A., LU, Z.X., SPONG, D.A., TODO, Y., AUSTIN, M.E., *et al.* 2019 Verification and validation of integrated simulation of energetic particles in fusion plasmas. *Nucl. Fusion* **59** (6), 066006.

TURNBULL, A.D., STRAIT, E.J., HEIDBRINK, W.W., CHU, M.S., DUONG, H.H., GREENE, J.M., LAO, L.L., TAYLOR, T.S. & THOMPSON, S.J. 1993 Global Alfvén modes: theory and experiment. *Phys. Fluids* B **5**, 2546–2553.

VAN ZEELAND, M.A., AUSTIN, M.E., GORELENKOV, N.N., HEIDBRINK, W.W., KRAMER, G.J., MAKOWSKI, M.A., MCKEE, G.R., NAZIKIAN, R., RUSKOV, E. & TURNBULL, A.D. 2007 Coupling of global toroidal Alfvén eigenmodes and reversed shear Alfvén eigenmodes in DIII-D. *Phys. Plasmas* **14**, 056102.

YU, L., FU, G.Y. & SHENG, Z.M. 2009 Kinetic damping of Alfvén eigenmodes in general tokamak geometry. *Phys. Plasmas* **16**, 072505.

ZONCA, F., CHEN, L., DONG, J.Q. & SANTORO, R.A. 2014 Theory on excitations of drift Alfvén waves by energetic particles. I. Variational formulation. *Phys. Plasmas* **21**, 072120.